ACS APPLIED MATERIALS & INTERFACES

Subscriber access provided by La Trobe University Library

Biological and Medical Applications of Materials and Interfaces

Biofunctional silk kirigami with engineered properties

Sayantan Pradhan, Leonardo Ventura, Francesca Agostinacchio, Meng Xu, Ettore Barbieri, Antonella Motta, Nicola Maria Pugno, and Vamsi K Yadavalli

ACS Appl. Mater. Interfaces, **Just Accepted Manuscript** • DOI: 10.1021/acsami.9b20691 • Publication Date (Web): 25 Feb 2020

Biofunctional silk kirigami with engineered properties

*Sayantan Pradhan, Leonardo Ventura, Francesca Agostinacchio, Meng Xu, Ettore Barbieri, Antonella Motta, Nicola M. Pugno *, Vamsi K Yadavalli **

S. Pradhan, Dr. M. Xu, Dr. V. K. Yadavalli
Department of Chemical and Life Science Engineering
Virginia Commonwealth University
601 W Main Street, Richmond VA, USA 23284

F. Agostinacchio, Prof. A. Motta
BIOtech Research Center
Department of Industrial Engineering
University of Trento, TN, Italy

Dr. E. Barbieri
Japan Agency for Marine-Earth Science and Technology
Center for Mathematical Science and Advanced Technology
Computational Science and Engineering Group
3173-25, Showa-machi, Kanazawa-ku, Yokohama-city, Kanagawa, 236-0001, Japan

Prof. N. M. Pugno
Laboratory of Bio-Inspired & Graphene Nanomechanics,
Department of Civil, Environmental and Mechanical Engineering,
University of Trento, TN, Italy
& Fondazione Edoardo Amaldi, Via del Politecnico snc, Rome, Italy

L. Ventura, Prof. N. M. Pugno
School of Engineering and Materials Science,
Queen Mary University of London, L, United Kingdom

* - Corresponding authors: nicola.pugno@unitn.it, vyadavalli@vcu.edu

Abstract

The fabrication of multifunctional materials that interface with living environments is a problem of great interest. A variety of structural design concepts have been integrated with functional materials to form biodevices and surfaces for health monitoring. In particular, approaches based on kirigami-inspired cuts can engineer flexibility in materials through the creation of patterned defects. Here, the fabrication of a biodegradable and biofunctional "silk kirigami" material is demonstrated. Mechanically flexible, free-standing, optically transparent, large-area biomaterial sheets with precisely defined and computationally designed microscale cuts can be formed using a single-step photolithographic process. Using modeling techniques, it is shown how cuts can generate remarkable "self-shielding" leading to engineered elastic behavior and deformation. As composites with conducting polymers, flexible, intrinsically electroactive sheets can be formed. Importantly, the silk-kirigami sheets are biocompatible, can serve as substrates for cell culture, and be proteolytically resorbed. The unique properties of silk kirigami suggest a host of applications as transient, "green", functional biointerfaces, and flexible bioelectronics.

Keywords: silk fibroin, kirigami, micropatterning, conducting polymer, flexible, biodegradable

1. Introduction

Producing flexible, thin, mechanically robust and compliant interfaces which perform in dynamic environments is an ongoing challenge.[1-2] Such multifunctionality can establish adaptive interfaces with the body.[3] From human-machine interfaces and soft robotics, to implantable devices and engineered tissues for regenerative medicine, material design and fabrication strategies have focused on capturing the mechanical compliance and biomimetic sensing of skin.[4-6] Various architectures have been proposed to impart functional conformability with biological tissues including meshes, cracks, prestressing, buckling, and serpentine designs.[7-8] Integrating biocompatibility and biodegradation can vastly expand the scope of synthetic "skins" for applications in biohybrid systems, soft matter electronics,[9], prosthetics,[10] wound healing, neural interfaces, and health monitoring *in situ*.[11-12] Across length scales, micropatterned and microstructured materials may be used for cell co-cultures and spatial control.[13-15] Recently, approaches building on principles borrowed from the Japanese paper arts such as origami and kirigami, have shown great promise.[16] Origami refers to folding ("*ori-*"), whereas kirigami involves cutting ("*kiri-*") of paper ("*-gami*"). Complex and functional objects using combinations of cutting, bending, and/or folding of diverse materials have been shown artistically and scientifically.[17]

Of interest is the use of kirigami-inspired cuts to transform materials towards multifunctional biointerfaces. While designed to enhance elasticity for traditionally stiff materials, kirigami architectures can transform intrinsically flexible and soft materials in interesting ways. For instance, mechanical properties at scales smaller than the cuts would not change, whereas effective properties at scales larger than the cuts would.[18] Substrates can be imbued with deformability

beyond the strain limits of pristine materials, allowing for multifunctionality e.g. stretchability, conformability to complex interfaces, conductivity, fault tolerance, biocompatibility, and reconfigurability. Out-of-plane deformations can enable reversible geometry changes, transforming between planar 2D and 3D.[8, 17, 19] Using computational tools, it is possible to predict and thereby precisely engineer, the operative behaviors under mechanical stresses.

Previously, kirigami cuts have been accomplished using subtractive methods including microscale laser cutting, [20] optical lithography,[21] etching (e.g. plasma, masked ion),[22] and macroscopic cutting (e.g. x-acto knives).[23] In addition to the traditionally used paper, elastomers (polydimethylsiloxane), metal foils, plastics (polyimide, polyethylene terephthalate, polyester films), and graphene-silk composite are among materials reported.[16-17] (Table S1 in the supporting information provides several recent examples). To impart conductivity, metal electrodes (Au, Ag, Pt, Al), indium tin oxide, carbon nanomaterials (nanotubes, graphene), conducting polymers, and 2D layered materials such as MoS_2, have been used.[7, 21, 24-25] A top-down, lithographic process was shown in a graphene oxide-polyvinyl alcohol nanocomposite with cuts formed using plasma etching through photoresist patterns deposited on the nanocomposite.[22] However, the use of fully biodegradable and biocompatible materials with kirigami strategies has not been shown.

For the first time, photolithographic fabrication of biofunctional, biodegradable silk kirigami via a facile, single step subtractive process is demonstrated. “Protein lithography” via photoreactive silk fibroin is utilized as a route to multiscale fabrication.[26-27] The biomaterial behaves as a negative-tone photoresist, crosslinking under UV irradiation. Whereas traditional kirigami uses cuts to form desired topologies, a photocurable material permits using photolithography to remove uncrosslinked material. This results in flexible, free-standing, optically transparent, macroscale sheets with precisely defined microscale cuts. Using finite element modeling and fracture

mechanics, a framework can be established to predict the stretching behavior of these films and their strength, as a function of different cut geometries. Cuts can bring about remarkable "self-shielding" leading to engineered elastic behavior. Silk-kirigami sheets are biocompatible, can serve as substrates for cell culture, and be proteolytically degraded. By doping with the conducting polymer polyaniline, intrinsically conducting silk kirigami films are demonstrated that are flexible, stretchable, and can be bent and twisted while retaining electrical properties. As mechanically-tunable cell scaffolds coupled with electrochemical properties, the use of bioinspired silk kirigami to form degradable and biocompatible, yet functional substrates facilitates advanced capabilities as engineered tissues and (bio)electronic interfaces.[11, 28-29]

2. Results and Discussion

2.1. Fabrication of flexible silk fibroin kirigami

Kirigami-inspired cuts/patterns using degradable and biocompatible polymers can add a new dimension to their function. Silk proteins form a versatile class of bioresorbable biomaterials for drug delivery, nanostructured scaffolds,[30] and recently, implantable bioelectronics, photonics, and bio-integrated devices.[31-32] Here, microfabrication of flexible, optically transparent kirigami films is realized using a light-reactive silk protein with a rapid, scalable process.[26, 33] Material subtraction or cutting is photolithographically accomplished in a single step process. The solution of photocrosslinkable (silk) fibroin in hexafluoroisopropanol was crosslinked by exposure through a photomask, resulting in complex patterns (Figure 1). As a negative-tone photoresist-like material, uncrosslinked material is developed, and the resulting free-standing silk kirigami sheet easily

peeled off. The sheets formed are stable in a wide range of solvents, and can be stored in air or water over several weeks without degradation.[27, 33]

The cuts have a high structural fidelity and spatial resolution demonstrating the scalability and accuracy of this photolithographic process to form micropatterns over large areas. SEM imaging shows ordered patterns of various complexities over a large area (cm scale) of flexible fibroin sheet (Figure 2b-f). They are optically transparent (Figure 2a), shown here with cuts – 50 μm wide, 500 μm long, enabling potential use in stretchable optics and transparent devices.[34]. Cuts down to ~10 μm using benchtop lithography can be easily formed, with nanoscale patterns possible using electron beam lithography.[35] The micro-cut kirigami films are mechanically robust and can be held, rolled or bent into various conformations without any loss in their physico-chemical-mechanical properties. Bending certain patterns such as branches, saddles, or chevrons result in interesting and useful microscale openings and out-of-plane deformations (Figure 2), (Figure S1). In an unanticipated result, it was observed that partial cuts, particularly at smaller feature sizes, could be formed by reducing the time of crosslinking. This results in films that can have engineered weakness along the partial cuts (Figure S2).

Films tens of μm thick are easily formed by controlling the amount of solution cast and the spin coating speed (films reported here are formed with thickness of 20-25 μm, confirmed by optical and electron microscopy). While the dry films are flexible but not compliant, moist films can be applied to, and readily conform to irregular surfaces (e.g. skin) (Figure 2g) without the need for adhesives. In comparison, a pristine film of similar size and thickness is quickly delaminated on bending the finger. The results show that moist silk kirigami films display enhanced adhesion to skin similar to earlier reported laser-cut PDMS.[36] Human skin is known to be stretchable to 75% strain, with surface strains ~55% at the knees.[37] The introduction of deformability in silk kirigami

sheets, with fracture-resistant openings to accommodate stretch allows highly conformable interfaces or attachment at interfaces.[38]

2.2. Tensile testing and finite-element modeling

Kirigami-based structural designs can achieve dynamic shaping towards stretchability and foldability.[39] Kirigami sheets possess a mechanical regime in which they are stretchable and soft in comparison to pristine (uncut) sheets.[40] The mechanical properties are dramatically affected by the presence of the cuts resulting in a desired large enhanced deformability but in undesired weakening, as predicted by fracture mechanics. Tensile testing was conducted on thin silk kirigami films with a simple, uniform slit geometry. Experimental values were obtained for two sets of cuts – 100 μm wide x 500 μm and 100 μm x 1000 μm long, as well as a branched geometry – 'Y'-cuts). Measurements were taken at a strain rate of 0.1 mm/s. Consistent with prior reports, pristine (uncut) silk films have a high breaking stress but fail at strains of ~ 7% (Figure S3).[41] In contrast, with a simple cut geometry, even completely dry silk kirigami films can be easily stretched to a strain of ~ 40% (Figure 3a – middle panel). The breaking strain recorded is typically below the strain at which the films completely fail. Even though some of the cuts tear, the entire structure does not come apart (Figure S4, S5). The stills from the tensile test with the point of failure (red-arrow) under load are shown in Figure S4).

The stress-strain response were then modeled using the Finite Element Method (FEM) software ABAQUS, which provides a high level of flexibility, reliability, and verifiability.[19, 22, 36] A parametric script was used to define different mechanical, geometrical boundary conditions. Input parameters used to perform a specific simulation varied geometry, material properties [Young's

modulus *E,* Poisson ratio *v,* density values of silk fibroin were used], and loading conditions. The mechanical constitutive model is elastoplastic with isotropic linear elasticity and linear hardening. The simulation allows the introduction of a "defect" in correspondence with the middle point of each cut which triggers the out-of-plane instability typically observed in kirigami structures. This used preliminary buckling analysis and a nonlinear quasi-static analysis under uniaxial tension. From Figure 3a, the excellent correlation and predictive ability of the simulations with the experimentally observed tensile behavior is noted, even at high strain. The stress visualizations at the crack tips are shown in Figure 4 for the slit geometry and the branched geometry under increasing loads (2-6 MPa). Complete details and videos of the simulations are provided in the Supporting Information. Using the predictive abilities of this FEM analysis, it is possible to *ab initio* design kirigami geometries for various applications.

2.3. Fracture mechanics and design of self-shielding cuts

A mathematical model was developed for the geometries tested to provide a framework for the strength of the silk kirigami films. The model is based on diamond-shaped arrays of "cracks" which are strikingly similar in geometry to the cut patterns.[42-43] Assumptions of linear elastic fracture mechanics, derived from the method of continuous dislocation distributions were applied. Briefly, considering the geometry shown in Figure 3 and 5, the kirigami shape factor Y depends on the half-length of the cuts (a) and the center-to-center horizontal (d) and vertical separation (b) between two consecutive cuts. Y accounts for the finiteness of the body with respect to the cut length. For example, a relatively short cut could act as a single central cut in an infinite plane, for which the shape factor is $Y = 1$. If the vertical spacing is large enough ($b/2a \rightarrow \infty$), then the shape factor may be approximated by a single row of collinear cuts (Figure 5b). Its general definition is:

$$Y = (1 - s) \qquad (1)$$

where $-\infty \leq s \leq 1$ is a calculated self-shielding factor dependent on the cut geometry (Table S2).[43] It is postulated that the cut overlaps protect each other resulting in a self-shielding mechanism in the kirigami films. If the vertical spacing is small enough ($b/2a \rightarrow 0$), this shielding mechanism occurs for overlapping rows of cuts (Figure 5a and 5c). Using these expressions, the critical strength σ^c of the various kirigami geometries and design self-shielding cuts can be estimated.

$$\sigma_c^{\infty} = \frac{K_{I_C}}{Y\sqrt{\pi a}} = \frac{K_{I_C}}{(1 - s\left(\frac{b}{2a}, \frac{d}{2a}\right))\sqrt{\pi a}} \qquad (2)$$

K_{I_C} is the critical stress intensity factor, estimated using properties of silk fibroin. Films with longer cuts have a larger cut overlap, resulting in effective shielding. For a cut length of 500 μm, the shape factor is Y_{500} = 0.65, while for 1000 μm cuts, the shape factor is Y_{1000} = 0.3. The ratio between critical strengths is therefore theoretically estimated to be 1.5, which favorably compares to the experimental value of ~1.2. A small discrepancy occurs because the technique of continuous dislocation distributions does not account for out-of-plane instability and the plastic hardening observed both experimentally and in FEM simulations. However, these values offer a satisfactory comparison, confirming the design of self-shielding cuts in silk kirigami.

The behavior of patterns with branched cuts can similarly be estimated. The stress intensity factor $K_{I_{\mathrm{br}}}$ of a symmetric single branched cut in an infinite medium was estimated using the continuous dislocation distribution technique.[42, 44] In this system, the length of the inclined branch *(c)* = length of the horizontal branch (*a)* = 200 μm and θ (inclination of the branch) = 60°. It is assumed that the interactions for a diamond-shaped array of straight cuts also apply to a diamond-shaped array of branched cuts. For branched cuts, the vertical separation is b = 866 μm, and horizontal

separation is d = 700 μm, corresponding to the condition of cut overlap. The shape factor is $Y_{br} \approx 0.65 = Y_{500}$. Therefore, the ratio of critical strength between the two kirigami with straight and branched cuts is ~ 1.7, which only slightly overestimates the strength of the kirigami with branched cuts (ratio ~1.4). Coupled with FEM simulations, such mathematical formulations therefore allow computationally design of self-shielding kirigami cuts with precisely engineered strength and stretchability.

2.4. Evaluation of biocompatibility and degradation

Substrates capable of supporting cell growth and providing topographical and spatial cellular control, can deliver insight into the dynamics of cell interactions, while providing for ordered cell-sheets, and cell-based biosensors.[45] Flexible polymeric meshes [46] and ultrathin polymeric films have been previously proposed as functional nanomembranes for directing cellular organization.[12] Precise micro and nanoscale surface cuts on a mechanically robust, stretchable biomimetic substrate provides fascinating opportunities to direct the behavior of cells, control cell morphology, interface with tissue, and provide shape-programmability.[47] The biocompatibility and non-cytotoxicity of the substrate biomaterial was earlier shown.[27] Cell viability was assessed using an MTT assay (Figure S6) showing that the silk kirigami films are conducive to viability and metabolic activity. To verify the potential for cell guidance on silk-kirigami, the mouse myoblast cell line C2C12 cells were studied. The kirigami films are robust enough to withstand sterilization procedures allowing for cell patterning (Figure 6). Two different conditions were explored to promote cell attachment - preconditioning with expansion media, and coating with human fibronectin. After 7 days of culture, the cell cytoskeleton and nuclei were stained with I-Fluor 488 and DAPI, respectively, and observed by confocal microscopy. Cells showed adherence to both

samples, but a higher and more homogeneous adhesion was observed on kirigami sheets preconditioned with expansion media (Figure 6b-d). This condition had the optimal proliferation rate and organization of the cells. Expectedly, the controls (TCP and uncut fibroin films) also showed good adhesion of cells (Figure S7). DAPI was completely absorbed by the films and used only to show the underlying organization of the cuts (blue films – Figure 6c).

The topographical features of the kirigami design clearly align adhesion along the cuts, guiding the cells via surface morphology. Moreover, the imaging highlights cell alignment on the edges of the cuts, and the formation of cytoskeletal bridges linking the sides of the holes (Figure 6b). Similar bridging was observed for fibronectin coated films (Figure S8). Such flexible, stretchable cell culture sheets can therefore be used for fundamental studies of 3D tissue models, where the cuts can guide cells, and the underlying sheets eventually degrade over time. Cuts also provide the opportunity to form sheets with communication and mass transfer between sheets. Biodegradable, free standing, flexible cell sheets can potentially be stacked to generate 3D multilayered structures, with conformal contact at the bio-interface.[48] By dissolving a fluorescent molecule within the fibroin solution, fluorescent kirigami in a variety of designs (Figure 6a) can be formed. In these films, the uniform green fluorescence is derived from FITC-dextran (MW 4 kDa).

An advantage in using silk kirigami in addition to its biocompatibility, is the ability of the materials to be controllably degraded in physiological environments. Proteolytic action results in degradation of the silk kirigami sheets leading to the complete loss of mass and structural integrity. An enzymatic biodegradation experiment was conducted on silk kirigami films incubated in PBS solution with or without protease (control) at 37^{o}C. Due to proteolytic biodegradation, a loss of weight was observed, and after 10 days, the films incubated in the enzyme broke down, whereas the control samples maintained their integrity and flexibility (Figure S9). This was consistent with

previous observations in which the biodegradability of fibroin based flexible devices can be tuned by controlling the degree of crosslinking and film thickness.[26, 33, 49] Stretchable devices and biointerfaces with precisely engineered lifetimes can therefore be fabricated using the kirigami films, which can be useful as flexible biomimetic cellular constructs for tissue regeneration, drug delivery platforms, and biosensors.

2.5. Conducting silk kirigami

While many soft materials are not potentially degradable or resorbable, conducting polymer composites with silk [50-51] and auxetic patches using chitosan,[52] have been used towards tissue-interfacing electronics, and e-textiles.[10, 39, 53] Graphene oxide biopaper was reported with high electrical conductivity.[54] It may be noted that this was primarily graphene oxide, with only 2-5% of silk fibroin to provide binding interactions. Silk-based bioelectronics have potential for advanced bio-applications, primarily as a bioresorbable substrate for ultrathin electronics.[31] Multifunctional kirigami with intrinsic electrical conductivity is demonstrated by incorporating the conducting polymer polyaniline (PANI) to form fully organic electroactive sheets. PANI has a high temperature resistance, environmental stability, and excellent electrical conductivity.[55] While PANI solubility is typically low in most solvents, it is soluble in the benign solvent formic acid which makes it suitable to form silk composites.[33] Initially, compositions were optimized for both electrochemical and mechanical properties. The presence of H-bonding between the benzene ring structures of the molecular backbone of PANI causes rigidity in the composite films making the films brittle at high concentrations.[55] High PANI concentrations impart a dark color to the films, making photolithography difficult (e.g. cuts < 100 μm are not easily formed). 1% PEG as a plasticizer was used to improve the flexibility of the silk sheets at optimal PANI concentrations

(11% w/w), resulting in mechanically robust and flexible films (Figure 7a).

Conducting kirigami films were made in a similar manner, via UV crosslinking through a photomask followed by development. The electrical conductivity was probed by forming connecting pads at the ends (Figure S10). Initially, kirigami films were compared to pristine (uncut) films of similar size. For the sake of simplicity, the linear cut geometry was tested. The difference in conductivity (Figure 7b) indicates that the properties of the films are a function of the cut geometry. Excellent conductive behavior was observed (μS conductance levels and linear behavior over a voltage range of -0.5 - + 0.5 V). The films (slit width 100 μm, length 500 μm, gap spacing – 500 μm and gap width 500 μm, 25 μm thick) retain their conductivity under stretch (Figure S11), although the conductance changes ~40% under 10% linear strain. An underlying PDMS slab was used as a support to precisely control the angle of bend and twist (Figure 7c, Figure S12). A bend of 50-55^{o} was performed in these experiments to simulate the bending at the knee.[37] The films themselves are stable and function independently of the support. A change in conductance from 3.03 μS to 2.35 μS (~22%) was observed in the film on 55^{o} bend. The conductance changes as a function of stretch and also bending, which indicates that the composites undergo conformational changes on mechanical deformation. However, the films remain conductive under twist and 180^{o} bend (Figure 7d) Coupled with the deformability and stretchability shown, these intrinsically conducting silk kirigami films can therefore be designed for skin-like devices, with a better understanding of the electrochemical behavior linked to the dynamics of deformation.[38] As bioinspired and degradable platforms that can be formed in a green fashion, this platform can go a long way towards addressing sustainability in bioelectronics.[56]

3. Conclusions

In summary, the fabrication of multifunctional silk kirigami films using a facile photolithographic technique is demonstrated. The kirigami films themselves are simultaneously extremely stretchable and robust thanks to self-shielding cuts, and can be formed at various thicknesses ranging from thin (ca. μm) to thick (10s of microns), as well as degradable. The cut geometries of these films can be easily engineered via light-assisted microfabrication, which permits the formation of complex, high resolution architectures at high throughput and scale. The computational FEM and theoretical fracture mechanics models guide and support the experimental findings, and provide insight into the modes of deformation and fracture including the presence of self-shielding cuts and influence of geometry. Critically, these silk kirigami films are biocompatible and display the ability to spatially direct cell growth along the cut geometry, while also being controllably biodegradable. It is also possible to modulate the electrochemical characteristics of the films by doping with the conducting polymer polyaniline. These results suggest that silk kirigami can provide exceptional bioinspired and biodegradable structures towards flexible and stretchable biodevices.

4. Experimental Section

Fabrication of micropatterned kirigami films using photocrosslinkable fibroin

Photocrosslinkable fibroin (referred to as fibroin protein photoresist or photofibroin) was prepared by the incorporation of photoreactive moieties to fibroin as reported earlier.[26] 7.5% (w/v) of photofibroin was dissolved in HFIP with 2.5% (w/v) photoinitiator (Irgacure 2959, BASF). The solution was drop cast on plain glass slides and air dried for 15 minutes to evaporate excess solvent.

Samples were crosslinked using 365 nm UV (Lumen Dynamics OmniCure 1000) at 20 mW cm^{-2}. Uncrosslinked areas (cuts) were developed by soaking in 1M LiCl/DMSO. Free-standing films were obtained by soaking developed films in de-ionized water to delaminate them from the glass support. Films were washed in water and stored in air or water. To form conducting fibroin films, polyaniline (PANI) emeraldine salt from p-toluenesulfonic acid (Alfa Aesar, Tewksbury, MA) (11 % w/w) and photofibroin were dissolved in formic acid. Similar fabrication steps were followed.

Electrochemical Characterization

Linear sweep voltammetry (LSV) was used to characterize the electrochemical properties of the silk-PANI kirigami films. The measurement was conducted by a Gamry Interface 1010E Potentiostat (Gamry Instruments, Warminster, PA). The scanning range of applied potential was from – 0.5 V to 0.5 V (over 1V) with a rate of 100 mV/s. The electrochemical data was analyzed using Gamry Echem Analyst software. Electrical connections were testing by connecting to a DC power source.

Tensile tests

Kirigami samples fixed on a paper frame with a window of 0.5 cm side. The tensile test was performed on an MTS 300 series tensile testing machine (MTS Systems Corporation, Eden Prairie, MN) equipped with a 50 N load cell. Measurements were taken at a strain rate of 0.1 mm/s and data was collected at a rate of 10 Hz. All other parameters are sample specific such as thickness, width and length. Typically, films were 20-25 μm thick.

Finite element modeling and simulation

The commercial software ABAQUS was used to compute the deformations of the kirigami films for the three patterns in Figure 3a. The mesh is composed of 6-node triangular thin shell elements

(STRI65) near the tips to limit elements distortion upon cut opening, and 8-node quadrangular thin shells (S8R5) for the rest of the domain. A convergence analysis through mesh refinement was conducted to ensure mathematical accuracy. The final ratio between average mesh size (and the width of the films was 560) and the cut width was 4. An elastoplastic isotropic linear elastic constitutive model, with linear hardening was used. The material properties are Young Modulus 248 MPa, Poisson ratio 0.3, yield stress 12.92 MPa, hardening coefficient 26.36 MPa. To stabilize the dynamic implicit simulations, artificial numerical damping is introduced (by setting the parameters $\alpha = -0.41421$, $\beta = 0.5$ and $\gamma = 0.91421$ in the Hilber-Hughes-Taylor time integration). Quasi-static conditions are ensured by monitoring the kinetic energy.

Cell culture experiments

Mouse muscle myoblast cells (C2C12) were expanded in medium consisting in DMEM high glucose (Euroclone), 10% Fetal Bovine serum (Euroclone), 1% antibiotic/antimycotic (Euroclone), 1% L-glutamine (Euroclone), and 1% sodium Pyruvate (GIBCO). Cells were cultured in 75 cm^2 flask at 37°C and 5% CO_2 in humidified atmosphere and expanded until 70% confluence was reached. For this experiment the cell passage was 16. Samples were pretreated by two different methods - one group was preconditioned with complete expansion medium at 37°C for 30 minutes, the other was incubated with human fibronectin (Sigma Aldrich) for 1 hour at 37°C. As a control silk fibroin sheets without cuts were used and preconditioned with complete expansion medium and with human fibronectin, as kirigami films. All samples were sterilized with 70% ethanol for 40 minutes and then washed twice with sterile PBS (Euroclone).

Morphological evaluation of adhered cells

Adhered cell morphology on kirigami sheets were studied by imagining by confocal microscopy

at day 7 after seeding using Nikon A1 Laser Microscope. Before confocal observations, samples were fixed with 4% PFA for 40 minutes, permeabilized with 0.2% Triton X-100 for 30 minutes. The nuclei and the cell cytoskeleton were stained with DAPI (Sigma-Aldrich) and I-Fluor 488 (Abcam), respectively, per the manufacturers' instruction.

Proteolytic degradation in vitro

Silk fibroin films can be proteolytically degraded over time in the presence of enzymes. In the present work, the degradation of silk kirigami films in the presence of protease (Protease XIV from *Streptomyces griseus,* ≥3.5 U mg^{-1}, Sigma Aldrich) was demonstrated. Films - 20 μm thick with 100 μm cuts (containing ~2.5 mg fibroin) were incubated in 5 mL protease (1 U mg^{-1} of protein) at 37 °C and the degradation was studied over 2 weeks. Note that this protease concentration is ~3x the prior used concentrations, resulting in a comparatively rapid degradation.[26, 33, 49] Another set of samples were incubated in PBS buffer under the same environment, which served as the negative control. The enzyme solution was replaced every 3 days to maintain protease activity. Samples from each set were taken out on different days, rinsed with DI water, and imaged under a microscope to record their degradation over time.

Supporting Information

Supporting information showing prior kirigami literature, additional images of the silk kirigami, MTT assay, cellular spreading, mathematical modeling, simulations, tensile behavior, and conductive silk kirigami are provided. Videos of the tensile simulations are shown.

Acknowledgements

This research was partly supported by funding from the National Science Foundation (CBET-1704435). SEM images were obtained at the VCU Nanomaterials Characterization Center.

NMP is supported by the European Commission under the Graphene Flagship Core 2 grant No. 785219 (WP14 "Composites") and FET Proactive "Neurofibres" grant No. 732344 as well as by the Italian Ministry of Education, University and Research (MIUR), under the "Departments of Excellence" grant L. 232/2016, the ARS01-01384-PROSCAN Grant and the PRIN-20177TTP3S.

EB is supported by JSPS KAKENHI Grant Number JP18K18065 and the Cross-Ministerial Strategic Innovation Promotion (SIP) Program for Deep Ocean Resources.

References:

1. Jeong, J. W.; Yeo, W. H.; Akhtar, A.; Norton, J. J.; Kwack, Y. J.; Li, S.; Jung, S. Y.; Su, Y.; Lee, W.; Xia, J., Materials and Optimized Designs for Human-Machine Interfaces via Epidermal Electronics. *Adv. Mater.* **2013,** *25*, 6839-6846.
2. Cai, P.; Hu, B.; Leow, W. R.; Wang, X.; Loh, X. J.; Wu, Y. L.; Chen, X., Biomechano-Interactive Materials and Interfaces. *Adv. Mater.* **2018,** *30*, 1800572.
3. Lendlein, A.; Trask, R. S., Multifunctional Materials: Concepts, Function-Structure Relationships, Knowledge-Based Design, Translational Materials Research. *Multifunct. Mater.* **2018,** *1*, 010201.
4. Lu, N. S.; Kim, D. H., Flexible and Stretchable Electronics Paving the Way for Soft Robotics. *Soft Robot* **2014,** *1*, 53-62.
5. Hammock, M. L.; Chortos, A.; Tee, B. C. K.; Tok, J. B. H.; Bao, Z., 25th anniversary article: The Evolution of Electronic Skin (E-Skin): A Brief History, Design Considerations, and Recent Progress. *Adv. Mater.* **2013,** *25*, 5997-6038.
6. Kim, D. H.; Lu, N. S.; Ma, R.; Kim, Y. S.; Kim, R. H.; Wang, S. D.; Wu, J.; Won, S. M.; Tao, H.; Islam, A.; Yu, K. J.; Kim, T. I.; Chowdhury, R.; Ying, M.; Xu, L. Z.; Li, M.; Chung, H. J.; Keum, H.; McCormick, M.; Liu, P.; Zhang, Y. W.; Omenetto, F. G.; Huang, Y. G.; Coleman, T.; Rogers, J. A., Epidermal Electronics. *Science* **2011,** *333*, 838-843.
7. Matsuhisa, N.; Chen, X.; Bao, Z.; Someya, T., Materials and Structural Designs of Stretchable Conductors. *Chem. Soc. Rev.* **2019,** *48*, 2946-2966.
8. Xu, S.; Yan, Z.; Jang, K.-I.; Huang, W.; Fu, H.; Kim, J.; Wei, Z.; Flavin, M.; McCracken, J.; Wang, R., Assembly of Micro/nanomaterials into Complex, Three-dimensional Architectures by Compressive Buckling. *Science* **2015,** *347*, 154-159.
9. Lu, T.; Finkenauer, L.; Wissman, J.; Majidi, C., Rapid prototyping for Soft-matter Electronics. *Adv. Funct. Mater.* **2014,** *24*, 3351-3356.
10. Chortos, A.; Liu, J.; Bao, Z., Pursuing Prosthetic Electronic Skin. *Nat. Mater.* **2016,** *15*, 937-950.
11. Feiner, R.; Dvir, T., Tissue–electronics interfaces: From Implantable Devices to Engineered Tissues. *Nat. Rev. Mater.* **2018**, *3*, 17076.

12. Fujie, T., Development of Free-standing Polymer Nanosheets for Advanced Medical and Health-care Applications. *Polym. J.* **2016**, *48*, 773-780.

13. Li, J.; Li, G.; Zhang, K.; Liao, Y.; Yang, P.; Maitz, M. F.; Huang, N., Co-Culture of Vascular Endothelial Cells and Smooth Muscle Cells by Hyaluronic Acid Micro-Pattern on Titanium Surface. *Appl. Surf. Sci.* **2013**, *273*, 24-31.

14. Meco, E.; Lampe, K. J., Microscale Architecture in Biomaterial Scaffolds for Spatial Control of Neural Cell Behavior. *Front. Mater.* **2018**, *5*, 2.

15. Lantigua, D.; Kelly, Y. N.; Unal, B.; Camci-Unal, G., Engineered Paper-based Cell Culture Platforms. *Adv. Healthc. Mater.* **2017**, *6*, 1700619.

16. Ning, X.; Wang, X.; Zhang, Y.; Yu, X.; Choi, D.; Zheng, N.; Kim, D. S.; Huang, Y.; Zhang, Y.; Rogers, J. A., Assembly of Advanced Materials into 3D Functional Structures by Methods Inspired by Origami and Kirigami: A Review. *Adv. Mater. Interfaces* **2018**, *5*, 1800284.

17. Xu, L.; Shyu, T. C.; Kotov, N. A., Origami and Kirigami Nanocomposites. *ACS Nano* **2017**, *11*, 7587-7599.

18. Chen, B. G.-g.; Liu, B.; Evans, A. A.; Paulose, J.; Cohen, I.; Vitelli, V.; Santangelo, C., Topological Mechanics of Origami and Kirigami. *Phys. Rev. Lett.* **2016**, *116*, 135501.

19. Vachicouras, N.; Tringides, C. M.; Campiche, P. B.; Lacour, S. P., Engineering Reversible Elasticity in Ductile and Brittle Thin Films Supported by a Plastic Foil. *Extreme Mech. Lett.* **2017**, *15*, 63-69.

20. Groeger, D.; Steimle, J., LASEC: Instant Fabrication of Stretchable Circuits Using a Laser Cutter. *Proceedings of the 2019 CHI Conference on Human Factors in Computing Systems,* Glasgow UK, **2019,** 1-14.

21. Blees, M. K.; Barnard, A. W.; Rose, P. A.; Roberts, S. P.; McGill, K. L.; Huang, P. Y.; Ruyack, A. R.; Kevek, J. W.; Kobrin, B.; Muller, D. A., Graphene kirigami. *Nature* **2015**, *524*, 204-207.

22. Shyu, T. C.; Damasceno, P. F.; Dodd, P. M.; Lamoureux, A.; Xu, L.; Shlian, M.; Shtein, M.; Glotzer, S. C.; Kotov, N. A., A Kirigami Approach to Engineering Elasticity in Nanocomposites through Patterned Defects. *Nat. Mater.* **2015**, *14*, 785-789.

23. Lamoureux, A.; Lee, K.; Shlian, M.; Forrest, S. R.; Shtein, M., Dynamic Kirigami Structures for Integrated Solar Tracking. *Nat. Commun.* **2015**, *6*, 8092.

24. Zheng, W.; Huang, W.; Gao, F.; Yang, H.; Dai, M.; Liu, G.; Yang, B.; Zhang, J.; Fu, Y. Q.; Chen, X., Kirigami-Inspired Highly Stretchable Nanoscale Devices Using Multidimensional Deformation of Monolayer MoS2. *Chem. Mater.* **2018,** *30*, 6063-6070.

25. Hu, K.; Gupta, M. K.; Kulkarni, D. D.; Tsukruk, V. V., Ultra-robust Graphene Oxide-silk Fibroin Nanocomposite Membranes. *Adv. Mater.* **2013,** *25*, 2301-2307.

26. Kurland, N. E.; Dey, T.; Kundu, S. C.; Yadavalli, V. K., Precise Patterning of Silk Microstructures Using Photolithography. *Adv. Mater.* **2013,** *25*, 6207-6212.

27. Xu, M.; Pradhan, S.; Agostinacchio, F.; Pal, R. K.; Greco, G.; Mazzolai, B.; Pugno, N. M.; Motta, A.; Yadavalli, V. K., Easy, Scalable, Robust, Micropatterned Silk Fibroin Cell Substrates. *Adv. Mater. Interfaces* **2019**, *6*, 1801822.

28. Muskovich, M.; Bettinger, C. J., Biomaterials-Based Electronics: Polymers and Interfaces for Biology and Medicine. *Adv. Healthc. Mater.* **2012**, *1*, 248-266.

29. Irimia-Vladu, M., "Green" electronics: Biodegradable and Biocompatible Materials and Devices for Sustainable Future. *Chem. Soc. Rev.* **2014**, *43*, 588-610.

30. Omenetto, F. G.; Kaplan, D. L., New Opportunities for an Ancient Material. *Science* **2010**, *329*, 528-531.

31. Hwang, S. W.; Kim, D. H.; Tao, H.; Kim, T. I.; Kim, S.; Yu, K. J.; Panilaitis, B.; Jeong, J. W.; Song, J. K.; Omenetto, F. G.; Rogers, J. A., Materials and Fabrication Processes for Transient and Bioresorbable High-Performance Electronics. *Adv. Funct. Mater.* **2013,** *23*, 4087-4093.

32. Tao, H.; Kainerstorfer, J. M.; Siebert, S. M.; Pritchard, E. M.; Sassaroli, A.; Panilaitis, B. J. B.; Brenckle, M. A.; Amsden, J. J.; Levitt, J.; Fantini, S.; Kaplan, D. L.; Omenetto, F. G., Implantable, Multifunctional, Bioresorbable Optics. *Proc. Natl. Acad. Sci. U.S.A* **2012**, *109*, 19584-19589.

33. Bucciarelli, A.; Pal, R. K.; Maniglio, D.; Quaranta, A.; Mulloni, V.; Motta, A.; Yadavalli, V. K., Fabrication of Nanoscale Patternable Films of Silk Fibroin Using Benign Solvents. *Macromol. Mater. Eng.* **2017**, *302*, 1700110.

34. Kim, K.; Park, Y. G.; Hyun, B. G.; Choi, M.; Park, J. U., Recent Advances in Transparent Electronics with Stretchable Forms. *Adv. Mater.* **2019**, *31*, 1804690.

35. Pal, R. K.; Yadavalli, V. K., Silk Protein Nanowires Patterned using Electron Beam Lithography. *Nanotechnology* **2018**, *29*, 335301.

36. Zhao, R.; Lin, S.; Yuk, H.; Zhao, X., Kirigami Enhances Film Adhesion. *Soft Matter* **2018**, *14*, 2515-2525.

37. Yamada, T.; Hayamizu, Y.; Yamamoto, Y.; Yomogida, Y.; Izadi-Najafabadi, A.; Futaba, D. N.; Hata, K., A Stretchable Carbon Nanotube Strain Sensor for Human-motion Detection. *Nat. Nanotechnol.* **2011**, *6*, 296-301.

38. Wang, S.; Oh, J. Y.; Xu, J.; Tran, H.; Bao, Z., Skin-inspired Electronics: an Emerging Paradigm. *Accounts Chem. Res.* **2018**, *51*, 1033-1045.

39. Wang, C.; Wang, C.; Huang, Z.; Xu, S., Materials and Structures toward Soft Electronics. *Adv. Mater.* **2018**, *30*, 1801368.

40. Isobe, M.; Okumura, K., Initial Rigid Response and Softening Transition of Highly Stretchable Kirigami Sheet Materials. *Sci. Rep.* **2016**, *6*, 24758.

41. Jiang, C.; Wang, X.; Gunawidjaja, R.; Lin, Y. H.; Gupta, M. K.; Kaplan, D. L.; Naik, R. R.; Tsukruk, V. V., Mechanical Properties of Robust Ultrathin Silk Fibroin Films. *Adv. Funct. Mater.* **2007,** *17*, 2229-2237.

42. Bilby, B. A.; Cottrell, A. H.; Swinden, K., The Spread of Plastic Yield from a Notch. *Proc. Roy. Soc. A.- Math Phy* **1963,** *272*, 304-314.

43. Delameter, W.; Herrmann, G., Weakening of Elastic Solids by Doubly-periodic Arrays of Cracks. In *Topics in Applied Continuum Mechanics*, Springer: 1974; pp 156-173.

44. Chen, Y.; Hasebe, N., New Integration Scheme for the Branch Crack Problem. *Eng. Fract. Mech.* **1995,** *52*, 791-801.

45. Feinberg, A. W.; Feigel, A.; Shevkoplyas, S. S.; Sheehy, S.; Whitesides, G. M.; Parker, K. K., Muscular Thin Films for Building Actuators and Powering Devices. *Science* **2007,** *317*, 1366-1370.

46. Gong, M.; Wan, P.; Ma, D.; Zhong, M.; Liao, M.; Ye, J.; Shi, R.; Zhang, L., Flexible Breathable Nanomesh Electronic Devices for On-Demand Therapy. *Adv Funct Mater* **2019**, *29*, 1902127.

47. Studart, A. R.; Erb, R. M., Bioinspired Materials that Self-shape through Programmed Microstructures. *Soft matter* **2014,** *10*, 1284-1294.

48. Haraguchi, Y.; Shimizu, T.; Sasagawa, T.; Sekine, H.; Sakaguchi, K.; Kikuchi, T.; Sekine, W.; Sekiya, S.; Yamato, M.; Umezu, M., Fabrication of Functional Three-dimensional Tissues by Stacking Cell Sheets *in vitro*. *Nat. Protoc.* **2012,** *7*, 850-858.

49. Pal, R. K.; Farghaly, A. A.; Wang, C.; Collinson, M. M.; Kundu, S. C.; Yadavalli, V. K., Conducting Polymer-silk Biocomposites for Flexible and Biodegradable Electrochemical Sensors. *Biosens. Bioelectron.* **2016,** *81*, 294-302.

50. Lund, A.; Darabi, S.; Hultmark, S.; Ryan, J. D.; Andersson, B.; Ström, A.; Müller, C., Roll-to-Roll Dyed Conducting Silk Yarns: A Versatile Material for E-Textile Devices. *Adv. Mater. Technol-Us* **2018,** *3*, 1800251.

51. Müller, C.; Hamedi, M.; Karlsson, R.; Jansson, R.; Marcilla, R.; Hedhammar, M.; Inganäs, O., Woven Electrochemical Transistors on Silk Fibers. *Adv. Mater.* **2011,** *23*, 898-901.

52. Kapnisi, M.; Mansfield, C.; Marijon, C.; Guex, A. G.; Perbellini, F.; Bardi, I.; Humphrey, E. J.; Puetzer, J. L.; Mawad, D.; Koutsogeorgis, D. C., Auxetic Cardiac Patches with Tunable Mechanical and Conductive Properties toward Treating Myocardial Infarction. *Adv. Funct. Mater.* **2018,** *28*, 1800618.

53. Lipomi, D. J.; Bao, Z., Stretchable and Ultraflexible Organic Electronics. *MRS Bull.* **2017,** *42*, 93-97.

54. Hu, K.; Xiong, R.; Guo, H.; Ma, R.; Zhang, S.; Wang, Z. L.; Tsukruk, V. V., Self-Powered Electronic Skin with Biotactile Selectivity. *Adv. Mater.* **2016,** *28*, 3549-3556.

55. Sen, T.; Mishra, S.; Shimpi, N. G., Synthesis and Sensing Applications of Polyaniline Nanocomposites: A Review. *RSC Adv.* **2016,** *6*, 42196-42222.

56. Torculas, M.; Medina, J.; Xue, W.; Hu, X., Protein-based Bioelectronics. *ACS Biomater. Sci. Eng.* **2016,** *2*, 1211-1223.

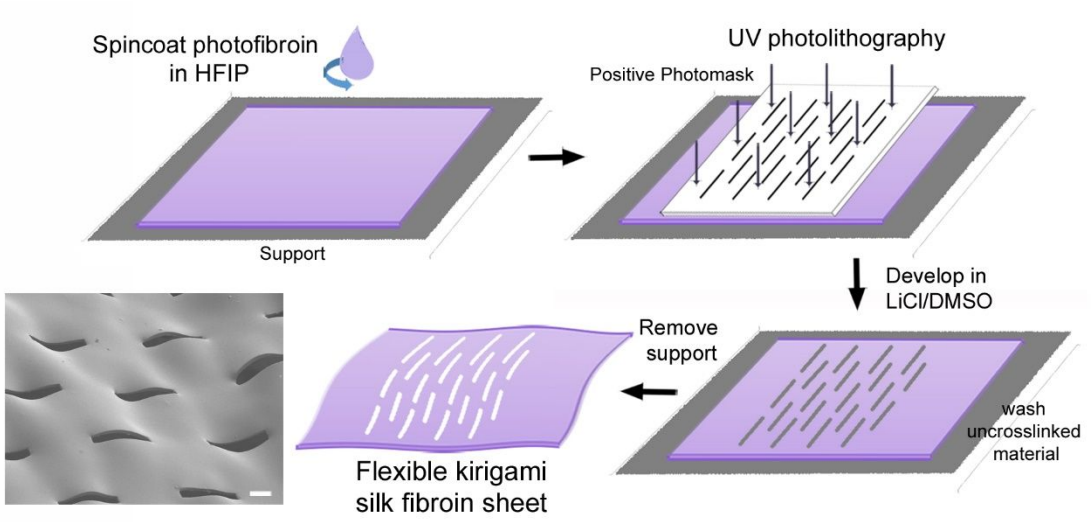

Figure 1: Schematic: Single step fabrication of kirigami cuts in silk fibroin films via photolithography.

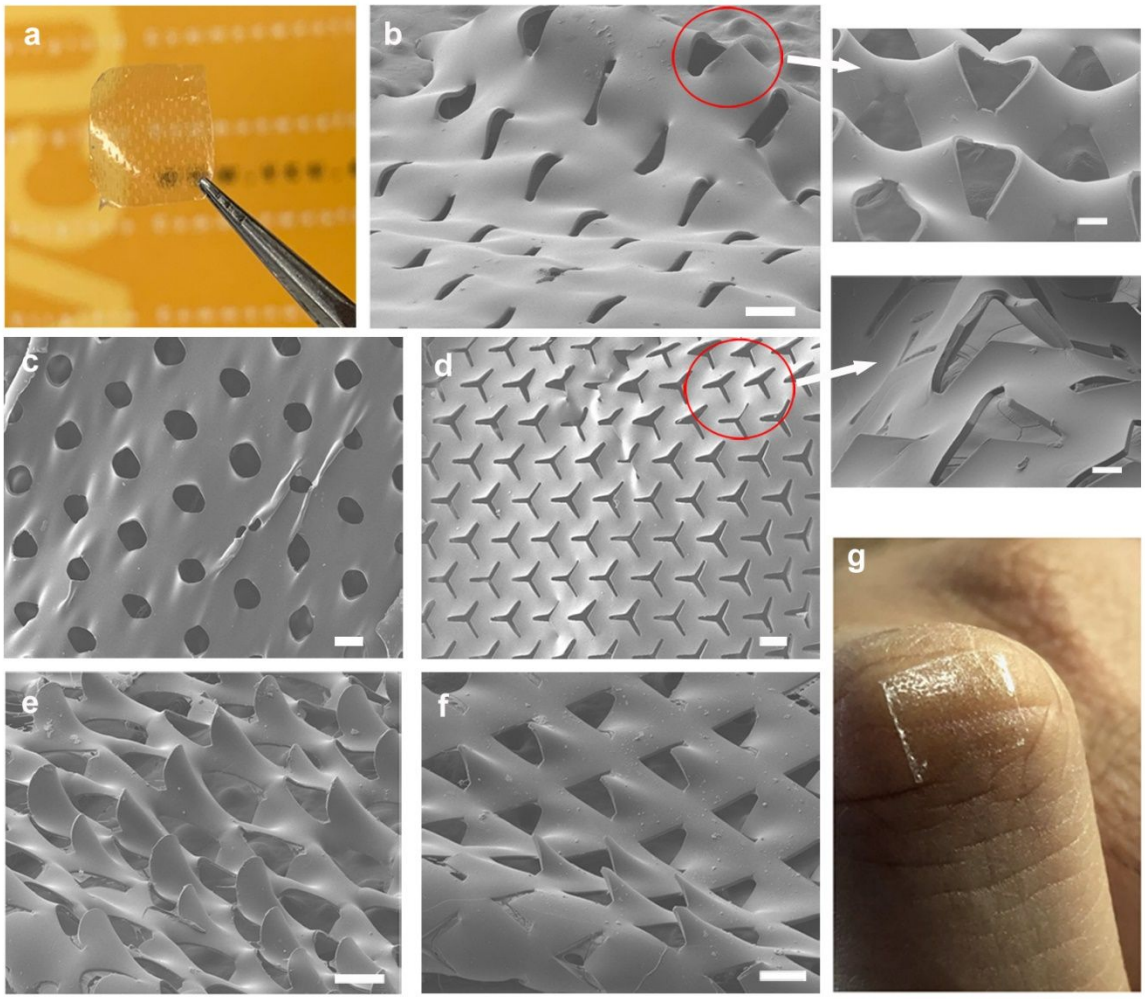

Figure 2: Imaging of silk kirigami **a**. Large scale silk kirigami films can be formed that are optically transparent (shown here are cuts 50 µm wide x 500 µm long). SEM images showing the diversity of geometries of cuts that can be formed using photolithography – **b**. linear cut geometry with 25 µm cuts, **c**. cross cuts that can be stretched biaxially, **d**. branched ('Y'-cuts), **e**. saddles **f**. chevrons. The top right insets show the out of plane deformation of the cuts. **g**. adherence of film shown in (a) to skin. The film is moist in this case and remains on during finger flexure. Scale bar on all images = 100 µm. Film thickness = 25 µm.

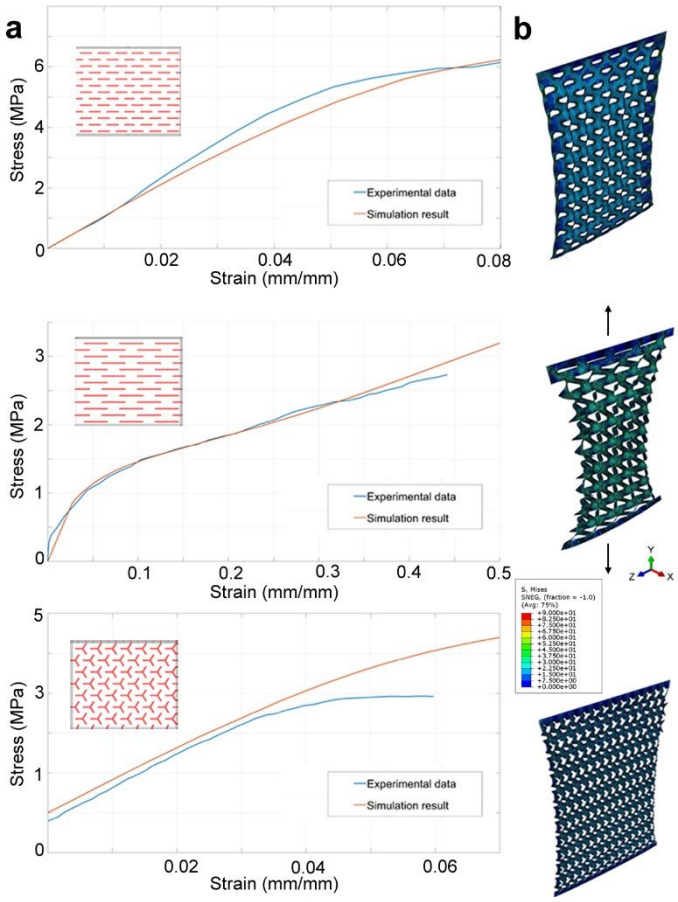

Figure 3: Mechanical behavior and simulations **a.** Stress-strain curves for different kirigami patterns: (top) shorter linear cuts (500 μm), (middle) longer linear cuts (1000 μm), and (bottom) branched cuts ('Y'-shapes) and their respective deformations – (red line: simulation result; blue line: experimental data). The contour plot reports the von Mises stress values. **b**. Visualization of the FEM modeling corresponding to the cuts shown. The scale bar shows increasing stress from blue to red.

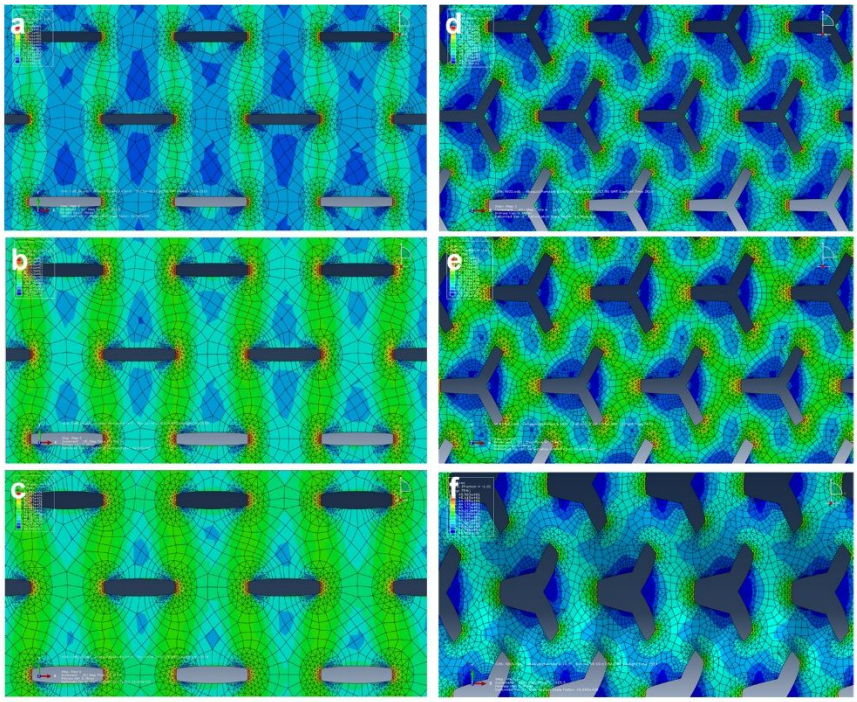

Figure 4: Visualization of the stress concentrations near the cut tips under increasing load conditions (top to bottom 2, 4 and 6 MPa) for a (a-c) slit geometry (500 μm length) and (d-f) branched (Y-shaped) cut geometry with 200 μm arm length.

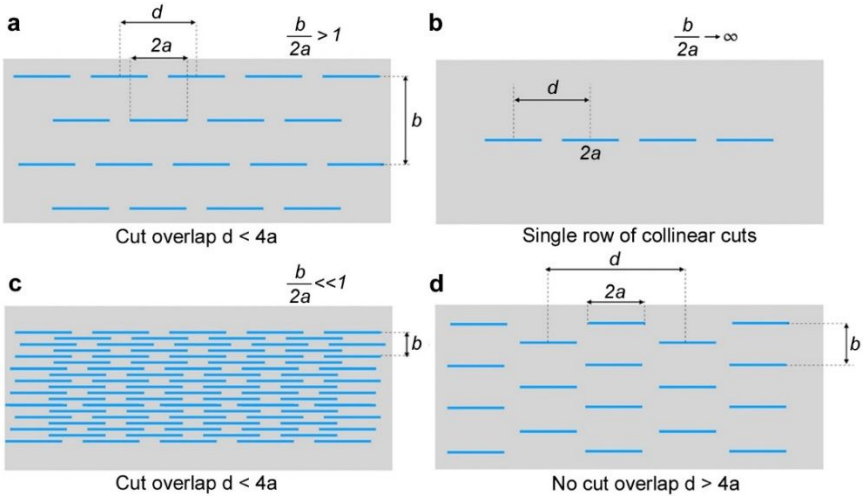

Figure 5: Kirigami patterns as **(a, c, d)** diamond-shaped array of cuts, and, **(b)** single row of collinear cuts.

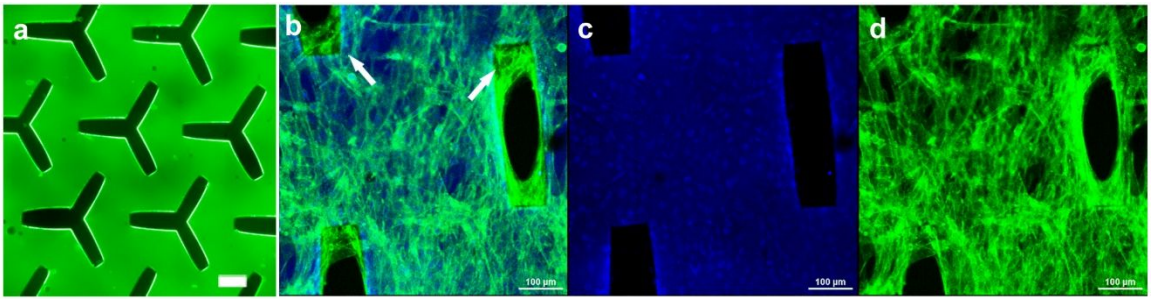

Figure 6: Functionality of silk kirigami **a**. Fibroin kirigami films can be loaded with fluorescent dyes (shown here – FITC-dextran MW 4 kDa). **b**. Adherence of C2C12 cells to the silk kirigami films 7 days after seeding. The arrows show the cytoskeletal bridges across the cuts. **c, d.** DAPI and actin staining.

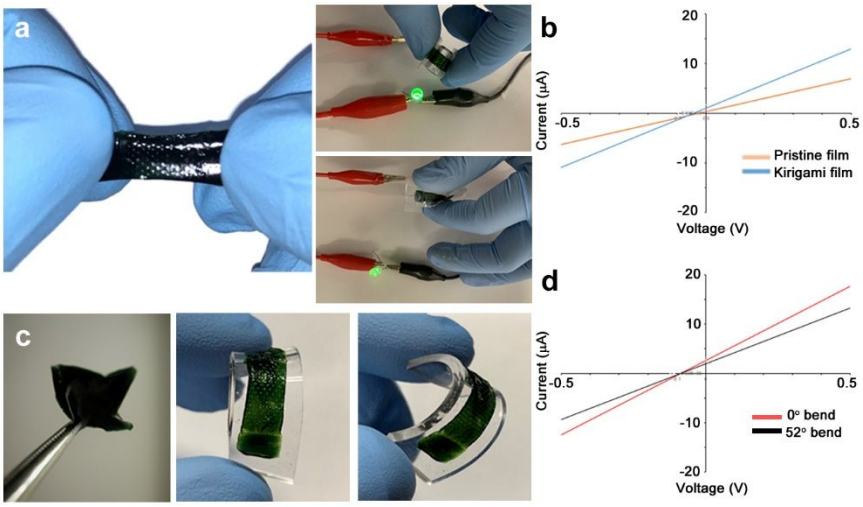

Figure 7. a. Electrically conducting, mechanically robust kirigami sheets that can be bent and twisted. Films are conductive enough to illuminate an LED under both bending and twisting. **b**. comparison of electrical behavior between a pristine (uncut) film and a kirigami film of similar size. **c**. Sheets can be folded and unfolded. A PDMS slab was used to provide support for measurement under bending. **d**. Comparison of behavior in relaxed (0^o) and bent (52^o) condition. Film thickness = 25 μm.

For Table of Contents Only